JOURNAL OF GEOPHYSICAL RESEARCH, VOL. 115, B04306, doi:10.1029/2009JB006438, 2010

Upper mantle deformation beneath the North American–Pacific plate boundary in California from *SKS* splitting

Mickael Bonnin,[1] Guilhem Barruol,[1] and Götz H. R. Bokelmann[1]

Received 6 March 2009; revised 27 August 2009; accepted 13 November 2009; published 8 April 2010.

[1] In order to constrain the vertical and lateral extent of deformation and the interactions between lithosphere and asthenosphere in a context of a transpressional plate boundary, we performed teleseismic shear wave splitting measurements for 65 permanent and temporary broadband stations in central California. We present evidence for the presence of two anisotropic domains: (1) one with clear E–W trending fast directions and delay times in the range 1.5 to 2.0 s and (2) the other closely associated with the San Andreas Fault system with large azimuthal variations of the splitting parameters that can be modeled by two anisotropic layers. The upper of the two layers provides fast directions close to the strike of the main Californian faults and averaged delay times of 0.7 s; the lower layers show E–W directions and delay times in the range 1.5 to 2.5 s and thus can be compared to what is observed in stations that require a single layer. We propose the E–W trending anisotropic layer to be a 150 to 200 km thick asthenospheric layer explained by the shearing associated with the absolute plate motion of the North American lithosphere. The shallower anisotropic layer ought to be related to the dynamics of the San Andreas Fault system and thus characterized by a vertical foliation with lineation parallel to the strike of the faults localized in the lithosphere. We also propose that the anisotropic layer associated with each fault of the San Andreas Fault system is about 40 km wide at the base of the lithosphere.

Citation: Bonnin, M., G. Barruol, and G. H. R. Bokelmann (2010), Upper mantle deformation beneath the North American–Pacific plate boundary in California from *SKS* splitting, *J. Geophys. Res.*, *115*, B04306, doi:10.1029/2009JB006438.

1. Introduction

[2] In the last decades, seismic anisotropy has become a powerful tool for mapping upper mantle deformation and for studying the dynamics of the lithosphere-asthenosphere system. Anisotropy, i.e., the physical property of a medium that induces variations in seismic wave velocities with the direction of propagation, is mostly related to rock microfracturing in the upper crust [e.g., *Crampin*, 1984] or to single-crystal intrinsic elastic properties associated with crystal-preferred orientation at greater depth such as in the lower crust [e.g., *Barruol and Mainprice*, 1993a] or in the upper mantle [e.g., *Mainprice and Silver*, 1993]. At upper mantle depths, seismic anisotropy results primarily from elastic anisotropy of rock-forming minerals, particularly olivine, which develop preferred orientations in response to tectonic stress and flow [e.g., *Nicolas and Christensen*, 1987; *Mainprice et al.*, 2000].

[3] Shear wave splitting is a direct effect of birefringence of the medium and therefore of seismic anisotropy: a shear wave crossing an anisotropic medium splits into two perpendicularly polarized shear waves that propagate at different velocities. From three-component seismic records, two parameters can be measured to quantify anisotropy: (1) the delay (δt) between the two split waves that depends on the thickness and on the intrinsic anisotropy of the medium and (2) the azimuth of the fast split wave polarization (ϕ), which is related to the orientation of the pervasive fabric in the anisotropic structure (foliation and lineation) or to fluid-filled microcracks at upper crustal levels.

[4] The San Andreas Fault (SAF) system is a transpressional, dextral strike-slip plate boundary that separates the Pacific plate from the North American plate [e.g., *Wallace*, 1990; *Bokelmann and Kovach*, 2000]. As it separates lithospheres with different nature and ages, it represents an area of major interest for studying the coupling between the Earth's envelopes, i.e., between the crust and the underlying lithospheric mantle and between the lithosphere and the underlying asthenosphere. The relatively simple and linear geometry of the SAF system and the dense seismological instrumentation of the area allow mapping of the deformation and its lateral and vertical variations beneath a major strike-slip plate boundary using shear wave splitting.

[5] In the last 2 decades, several studies have already focused on *SKS* splitting in California [*Ozalaybey and Savage*, 1994; *Silver and Savage*, 1994; *Ozalaybey and Savage*, 1995; *Hartog and Schwartz*, 2000, 2001; *Polet and Kanamori*, 2002]. These works evidenced regional variations in the

[1] Géosciences Montpellier, Université Montpellier II, CNRS, Montpellier, France.

0148-0227/10/2009JB006438

seismic parameters, particularly between stations close to the fault and those farther east, near the Sierras. In eastern California, directions of ϕ were described as trending mostly E–W, whereas near the SAF, fast split shear waves are trending NW–SE and are characterized by larger variations of ϕ with the wave back azimuths. *Silver and Savage* [1994] were the first to model these azimuthal variations in terms of two anisotropic layers for a set of stations close to the SAF: they found that an upper layer with a fast split direction close to the fault strike (ϕ_1 = 50°W), overlying a lower layer with E–W direction (ϕ_2 = 90°E), could explain the observed back azimuthal variations in ϕ and δt. *Ozalaybey and Savage* [1994] proposed a similar model for station BKS and other stations close to the SAF with $\phi_1 = 45 \pm 22$°W and $\phi_2 = 90 \pm 27$°E [*Ozalaybey and Savage*, 1995], with a close correlation between the fast azimuth and the strike of the faults. *Polet and Kanamori* [2002] explained the observed variations of the anisotropic parameters in terms of heterogeneity beneath the faults instead of models of two anisotropic layers. In all the papers dealing with models of two anisotropic layers, the different authors agree on the fact that the upper layer is closely related to the fault dynamics and with the associated shear. The origin of the deeper anisotropic layer is more debated, but it is generally associated with a regional asthenospheric flow. *Hartog and Schwartz* [2001] proposed the regional anisotropic layer to be related with absolute motion of the Sierra Nevada–Great Valley block, whereas *Ozalaybey and Savage* [1995] and *Polet and Kanamori* [2002] prefer to explain the regional fast axis directions pattern by postsubduction processes.

[6] The present paper takes advantage of the dense seismic coverage that has recently become available, and especially the recently acquired data from USArray, to better constrain the deformation associated with the plate boundary, as well as that induced by the relative motion between the plate and the convective mantle. The aim of this work is therefore to tackle the lateral and vertical extent of the deformation beneath the SAF system to elucidate the relations between the lithosphere and the underlying upper mantle for the various strike-slip faults accommodating the large-scale relative motion. The USArray experiment provides us an updated map of mantle deformation, even though these temporary deployments provided not more than 2 years of data each, while the regional broadband networks (e.g., Berkeley Digital Seismic Network (Berkeley network), California Integrated Seismic Network (Caltech)) now have stations with much more than 10 years of data. Permanent networks provide enough data to improve the back azimuthal coverage and to go further in the characterization of the complexity of the anisotropic structure.

[7] We focus our investigation on the area extending from the Pacific coast in the west to the Nevada border in the east and from N35° in the south to the Mendocino Triple Junction in the north. This is motivated by the fact that the SAF system is characterized by a relatively linear structure in this zone and that such a relatively simple geometry should permit discriminating between deformation related to the fault itself and deeper deformation. After a brief description of the data and method used in this work, we describe the individual and average results from the scale of the station to the regional scale. Section 4 discusses the various possible origins of the upper mantle anisotropies and their vertical and lateral locations.

2. Data and Methods

[8] In order to update the anisotropy map of the Californian upper mantle, we analyzed the complete data set provided by 65 broadband stations. These comprise 25 permanent stations of the Berkeley network in the northern part of the study area, 8 from Caltech in the southern part and 1 from the Geoscope network; we also used data from 28 temporary stations from the Transportable Array of the USArray experiment that provide a dense network with a station spacing of about 50 km, increasing considerably the spatial resolution. Finally, we used three stations from the California Transect experiment. Station locations are shown in Figure 1a and are also listed in Table 1.

[9] We analyzed *SKS* waveforms and performed shear wave splitting measurements at these 65 stations. In order to observe distinct, high signal-to-noise ratio *SKS* and *SKKS* phases, we systematically selected events with magnitudes (M_w) larger than 6.0 occurring at epicentral distances in the range of 85° to 120°. We obtained between 100 and 1000 events fitting our criteria at each station. Event origin times and locations were taken from the National Earthquake Information Center preliminary determination of epicenters catalog (U.S. Geological Survey). The phase arrivals were computed using the IASP91 Earth reference model [*Kennett and Engdahl*, 1991]. As an example, the events selected at station BKS (Figure 1b) show the rather good back azimuthal coverage that can be obtained in this area from permanent seismological stations.

[10] For each selected event, we measured the two splitting parameters, i.e., the azimuth of the fast axis ϕ and the delay time δt between the fast and slow components of the two split shear waves by using the SplitLab software [*Wüstefeld et al.*, 2008]. This software developed under the Matlab environment is freely available at http://www.gm.univ-montp2.fr/splitting/ and is particularly well suited to processing large amounts of data while preserving an event-by-event approach and helping the user in the fastidious tasks of data preprocessing and in the results analysis and diagnostic. It simultaneously utilizes three different techniques: (1) the rotation-correlation method [*Bowman and Ando*, 1987] to maximize the cross correlation between the radial and transverse component of the *SKS* phase, (2) the minimum energy method [*Silver and Chan*, 1991] to minimize the energy on the transverse component, and (3) the minimum eigenvalue method [*Silver and Chan*, 1991].

[11] We performed 1832 individual splitting measurements of which 1393 were nonnull measurements. The splitting parameters (ϕ, δt) are reported in Data Set S1 of the auxiliary material, together with the phase used, the back azimuth and angle of incidence of the selected events, and the error bars determined from the 95% confidence interval in the (ϕ, δt) domain.[1] We ascribe a quality factor for each measurement (good, fair, or poor) depending on the signal-to-noise ratio of the initial waveform, the correlation between the fast and slow shear waves, the linearization of the polar-

[1] Auxiliary materials are available at ftp://ftp.agu.org/apend/jb/2009jb006438.

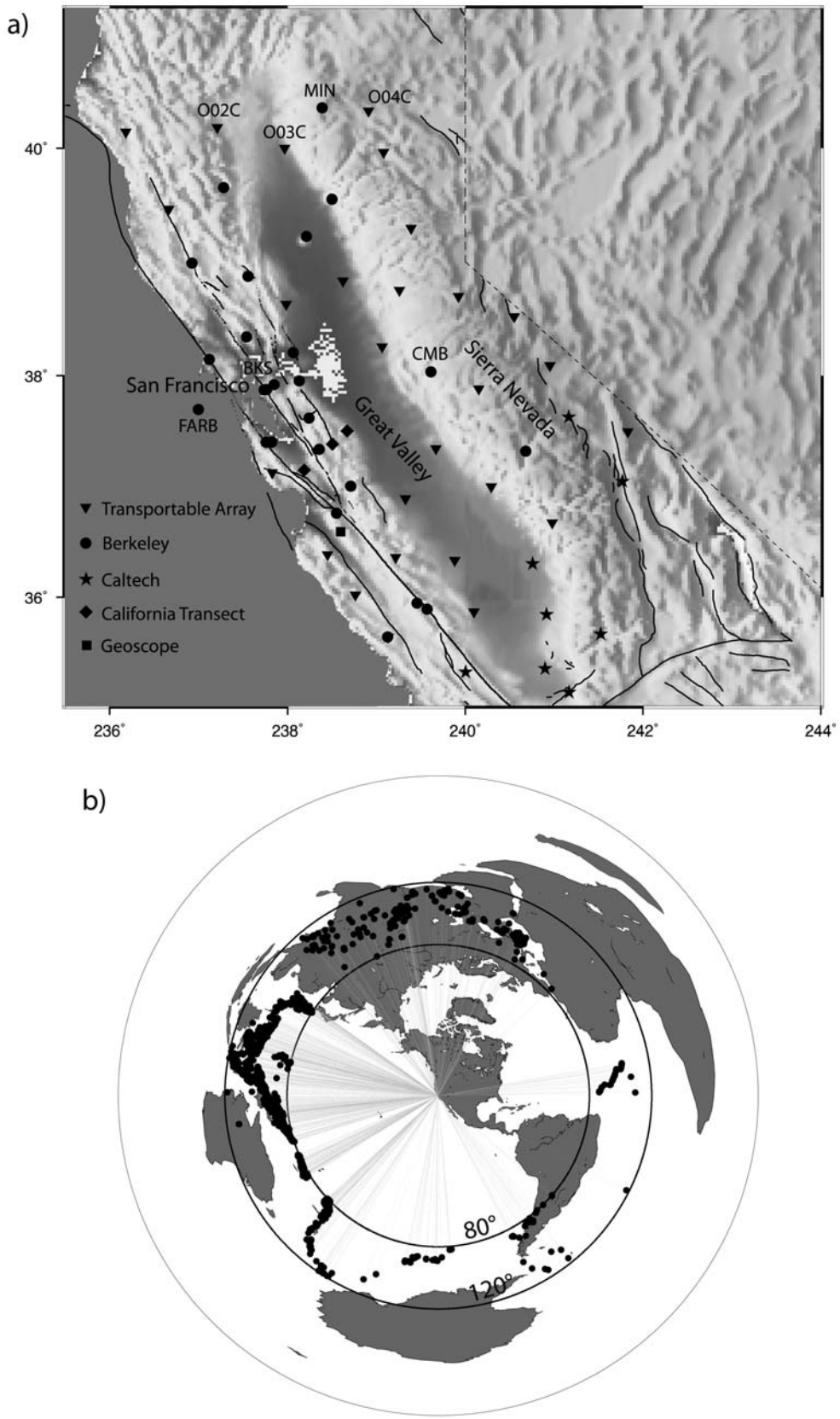

Figure 1. (a) Location of the broadband seismic stations used in this study. BKS, CMB, FARB, MIN, O02C, and O04C are stations cited in this study. Black lines show major faults of the San Andreas Fault (SAF) system. (b) Locations of the events selected at BKS station (magnitude greater than 6.0, occurring between 80° and 120° of epicentral distance); the projection preserves the back azimuthal coverage in the California region.

Table 1. Station Locations Together With the Number of Measurements Performed for Each Station[a]

Station	Latitude (deg)	Longitude (deg)	Number of Measurements				
			Total	Good	Fair	Poor	Nulls
ARV	35.127	−118.830	6	1	4	1	2
BAK	35.344	−119.104	15	4	4	2	5
BDM	37.954	−121.866	53	15	15	3	20
BKS	37.876	−122.236	68	22	23	16	7
BNLO	37.131	−122.173	17	3	9	2	3
BRIB	37.919	−122.152	24	8	13	1	2
BRK	37.874	−122.261	39	21	14	1	3
CMB	38.035	−120.387	164	48	50	25	41
CVS	38.345	−122.458	50	12	22	11	5
FARB	37.698	−123.001	28	17	3	1	7
FERN	37.153	−121.812	17	6	4	5	2
GASB	39.655	−122.716	10	2	2	1	5
HAST	36.389	−121.551	13	2	7	2	2
HELL	36.895	−120.674	24	6	9	2	7
HOPS	38.993	−123.072	72	17	27	20	8
ICAN	37.505	−121.328	15	5	5	3	2
ISA	35.663	−118.474	20	5	6	2	7
JRSC	37.404	−122.239	55	12	15	11	17
KCC	37.324	−119.319	100	35	37	15	13
LAVA	38.755	−120.740	26	7	7	2	10
MCCM	38.145	−122.880	10	4	2	1	3
MHC	37.342	−121.643	75	14	31	18	12
MIN	40.346	−121.607	20	2	5	1	12
MLAC	37.630	−118.836	16	6	9	0	1
MNRC	38.879	−122.443	19	1	9	2	7
O01C	40.140	−123.820	1	0	0	0	1
O02C	40.177	−122.788	7	3	2	1	1
O03C	39.997	−122.032	7	0	1	1	5
O04C	40.320	−121.086	14	7	4	1	2
O05C	39.962	−120.918	13	3	5	0	5
ORV	39.555	−121.500	114	24	26	8	56
P01C	39.469	−123.336	7	2	4	0	1
P05C	39.303	−120.608	14	4	3	1	6
PACP	37.008	−121.287	38	19	7	4	8
PKD	35.945	−120.542	41	12	20	3	6
PKD1	35.889	−120.426	14	5	4	0	5
POTR	38.203	−121.935	25	4	8	5	8
Q03C	38.633	−122.015	9	4	3	1	1
Q04C	38.834	−117.182	18	2	7	1	8
R04C	38.257	−120.936	32	12	11	1	8
R05C	38.703	−120.076	17	11	3	0	3
R06C	38.523	−119.451	14	10	4	0	0
R07C	38.089	−119.047	12	6	4	1	1
RAMR	35.636	−120.870	27	2	14	3	8
RCT	36.305	−119.244	5	2	0	0	3
S04C	37.505	−121.328	13	8	3	1	1
S05C	37.346	−120.330	24	10	8	2	4
S06C	37.882	−119.849	16	3	7	1	5
S08C	37.499	−118.171	17	12	4	0	1
SAO	36.764	−121.447	99	22	26	32	19
SAVY	37.389	−121.496	10	2	6	2	0
SCZ	36.598	−121.403	73	16	19	20	18
SMM	35.314	−119.996	28	6	3	9	10
STAN	37.404	−122.175	9	3	4	0	2
SUTB	39.229	−121.786	10	1	2	0	7
T05C	38.896	−120.674	6	1	3	1	1
T06C	37.007	−119.709	23	9	11	0	3
TIN	37.054	−118.230	27	7	17	1	2
U04C	36.363	−120.783	17	2	9	1	5
U05C	36.336	−120.121	8	1	6	0	1
V03C	36.021	−121.236	14	3	7	0	4
V04C	35.636	−120.870	15	1	7	0	7
V05C	35.867	−119.903	8	1	4	2	1
VES	35.841	−119.085	6	1	2	2	1
WENL	37.622	−121.757	22	8	11	0	3

[a]Good, fair, and poor are quality indicators assigned to measurements, where splitting is observed; whereas nulls are measurements where no splitting is apparent.

ization on the transverse component, the linear pattern of the particle motion in the horizontal plane after correction, and the size of the 95% confidence region. As SplitLab provides measurements performed with both the rotation-correlation (RC) method [*Bowman and Ando*, 1987] and the minimum energy method [*Silver and Chan*, 1991], the final quality also depends on the similarity between the two methods. Good measurements, such as the one shown in Figure 2 (event 1993.219.00 recorded at station CMB), satisfy the following conditions: (1) high initial wave signal-to-noise ratio, (2) good correlation between fast and slow shear waves, (3) good linearization of the polarization of the transverse component, (4) small confidence region, and (5) good correlation between the RC and minimum energy methods. This example clearly shows strong energy on the transverse component (T) of the initial seismogram, and the elliptical particle motion in the T-Q plane normal to the ray is well linearized after anisotropy correction [see *Wüstefeld et al.*, 2008]. Fair measurements fit at least four of these conditions; the other ones are poor measurements. This qualitative approach is very useful for analyzing and sorting the final results. Filtering was manually applied depending on characteristics of each seismogram in order to keep the largest amount of signal as possible. When necessary, i.e., when long-period and/or high-frequency noise level was present, they were band-pass filtered using various combinations of corner frequencies (typically between 0.01 and 0.2 Hz, as shown in Data Set S1 of the auxiliary material).

[12] In addition to the nonnull measurements, we observed 439 "nulls," i.e., event-station pairs devoid of energy on the transverse component of the seismogram suggesting that the *SKS* wave had not been split. This may happen in three kinds of situations: either (1) when the medium is isotropic; (2) when the incoming *SKS* wave is polarized parallel to the slow or the fast direction in the anisotropic medium; or (3) finally, in cases of two anisotropic layers with orthogonal symmetry axes beneath the station and with similar delay times in each layer, when the upper layer "removes" the delay acquired in the lower layer. We reported null measurements in Data Set S2 of the auxiliary material. We also ascribe quality to these measurements mostly depending on the presence of energy on the transverse component but also on the signal-to-noise ratio (SNR), on the linearity of the particle motion, and on the valley shape of the confident area. Good nulls are characterized by high SNR on the radial component and no energy on the transverse component; fair are measurements where there is some energy on the transverse component but not enough to measure splitting.

3. Results: Seismic Anisotropy Beneath Central California

3.1. Individual Splitting Measurements

[13] Figure 3a presents the whole set of individual splitting measurements that we performed in central California, plotted at each respective station. Figure 3b plots the back azimuth of the events that produced null splitting measurements. At large scale, fast axis directions show a regional clockwise rotation between values approximately NE–SW to E–W in the Sierra Nevada and values more NW–SE close to the Pacific coast. In the northern part of the map in

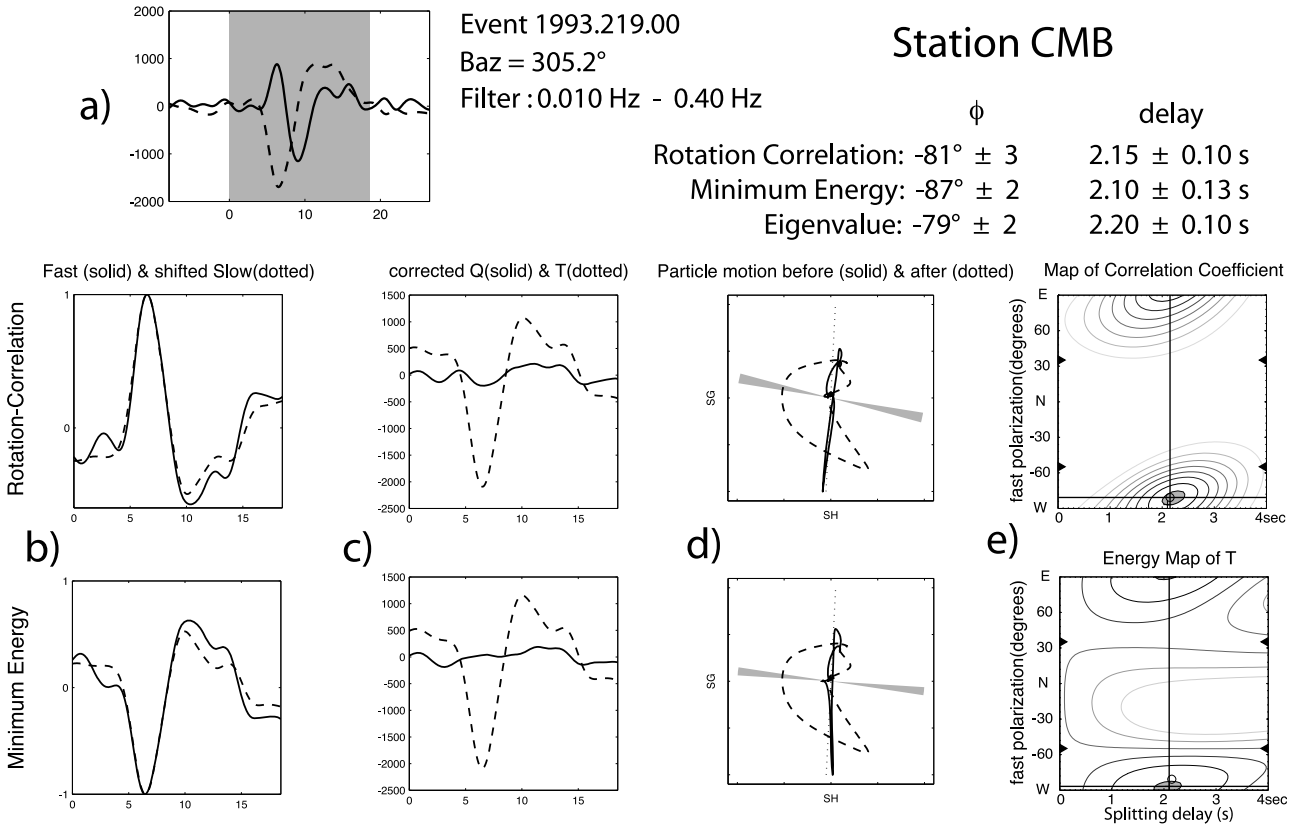

Figure 2. Example of a good splitting measurement (event 1993.219.00) at station CMB. (a) Initial seismogram before analysis (dashed line, radial component; solid line, transverse component; gray zone, calculation window). (b) Seismogram rotated in fast and slow orientations (dashed line, fast component; solid line, shifted slow component). (c) Anisotropy-corrected components (dashed line, radial component; solid line, transverse component). (d) Particle motion before (dashed line) and after (solid line) correction. (e) Splitting measurement result with 95% confidence region (gray zone); lines give values of splitting delay and fast direction. This example is characterized by an E–W trending fast anisotropic direction (N087°E) and by a 2.0 s delay time.

Figure 3a, three stations (O02C, MIN, and O04C (see Figure 1a for locations)) show a different trend with fast polarization directions going approximately E–W in the Sierra to clear NE–SW in the west. Null back azimuths are consistent with those observations: most nulls are observed along azimuths subparallel or perpendicular to the fast polarizations (see Figure 3). The splitting directions for the south of the studied area show strong variations of anisotropic parameters with a few measurements that can be partly explained by a lower signal-to-noise ratio at those stations.

[14] The general pattern is consistent with that of *Polet and Kanamori* [2002], who also observed an apparent clockwise rotation between eastern and western California. The present study, however, presents many more splitting measurements and fills several gaps of splitting observations that existed in central California, especially in the Great Valley area. A difference, with respect to *Polet and Kanamori* [2002], is that we observe strong variations for both ϕ and δt values at stations close to the SAF. This difference may be due to the fact that we processed more data than in their study. The directions of fast polarization obtained for the northern stations seem to be less N–S than in our study, doubtless caused by a smaller number of measurements.

3.2. Spatial Variations of Anisotropic Measurements

[15] As in previous studies, our observations indicate that central California seems to be characterized by two different regions regarding the degree of scatter of the anisotropic parameters. Stations in the vicinity of the SAF system are characterized by strong scatter in both the fast polarization directions and delay times, whereas stations located in the eastern and northern areas are characterized by much more homogeneous splitting directions, with values ranging between NE–SW and E–W. In order to illustrate this different anisotropic behavior, we present the individual anisotropic parameters in Figure 4 as a function of event back azimuth at station CMB in the Sierra Nevada and at station BKS on the SAF (see Figure 1 for locations).

[16] Our observations at CMB do not show strong and consistent variations in the splitting parameters with back azimuth. Even though back azimuthal coverage is not complete, we observe a rather good coherence of the fast polarization directions (Figure 4a) and delay times (Figure 4b) over the different azimuths. The absence of back azimuthal variation of the anisotropic parameters suggests a rather simple single-layer anisotropic structure beneath this station and allows us to determine the average ϕ as δt values for station CMB. These are well defined and N084°E

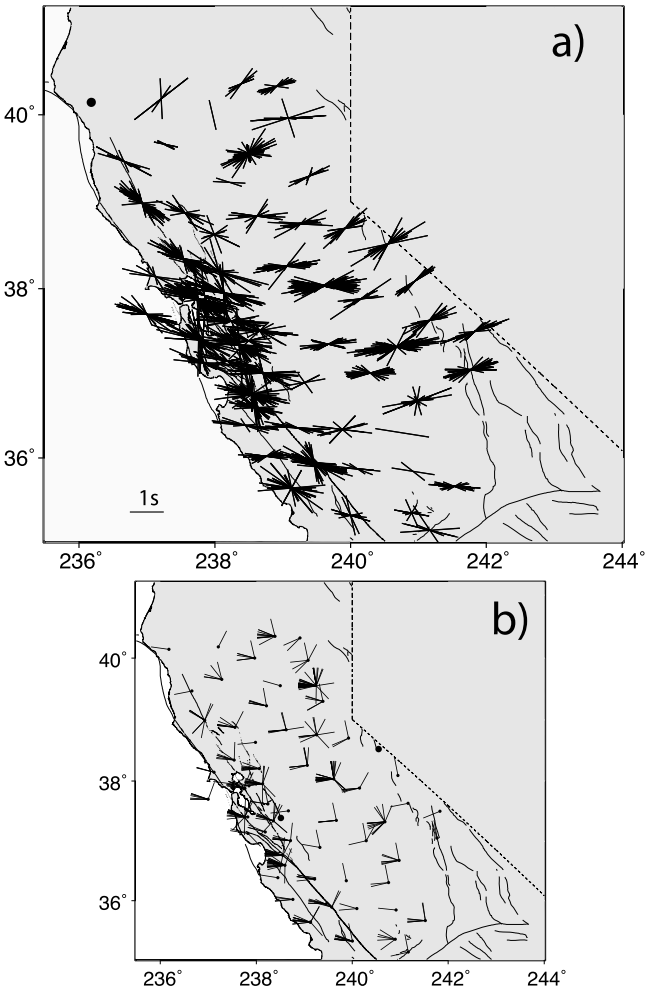

Figure 3. (a) Individual splitting measurements plotted at each station; the azimuth of each segment represents the direction of the fast split shear wave and the length of the segment the delay time. Black dot represents station which yielded no splitting measurement. (b) Null measurements observed at each station; directions of each segment represent the back azimuth of the events that produced nulls. Black dots are stations where no nulls were observed.

and 1.77 s, respectively. Such an averaging has been performed at every station where no coherent back azimuthal variation of ϕ and δt was observed; these values are reported in Table 2. Interestingly, all the stations characterized by a weak scatter in the splitting parameters give fast polarization directions ranging from N060°E to E–W and delay times in the range 1.0 to 2.0 s, with an average close to 1.5 s. All these stations are within and to the east of the Great Valley, and they define a zone in the Sierra where splitting parameters values seem homogeneous.

[17] Station BKS is close to the SAF and is representative of the western stations. Figures 4c and 4d present the clear and strong back azimuthal variations of ϕ in the range −60°E to −10°E and of δt in the range 0.8 to 3.2 s. These back azimuthal variations are clearly not random but well organized. Because of the large number of data, we obtain well-constrained back azimuthal variations of the anisotropic parameters that evidence a $\pi/2$ periodicity for both ϕ and δt, although the sparse azimuthal window results from the fact that most measurements have been performed from events coming from the west. Interestingly, 15 other stations located along the SAF system in central California present very similar patterns of variation in their anisotropic parameters.

3.3. Modeling of Two Anisotropic Layers

[18] Following *Silver and Savage* [1994], *Ozalaybey and Savage* [1994, 1995], *Barruol and Hoffmann* [1999], or *Hartog and Schwartz* [2001], we suggest that such back azimuthal variation could result from the presence of two anisotropic layers beneath these stations. This is motivated by the well-developed $\pi/2$ periodicity of the anisotropic parameter variations in our data, which is well explained by the presence of two anisotropic layers beneath a seismic station. We propose below a modeling approach to constrain the possible geometries of these anisotropic layers that may explain our observations.

[19] A shear wave propagating successively through two anisotropic layers is split twice and should generate four quasi-shear waves that should be observed at the receiver. Because the signal period typically ranges from 8 to 30 s and the amplitude of the delay times is around 1 s, the split waves are not individualized but overlapping each other; therefore, only apparent splitting parameters can be deduced from the waveform analysis. As described by *Silver and Savage* [1994], one can, however, calculate the theoretical apparent ϕ and δt variations as a function of the event back azimuth by direct modeling, keeping in mind that it is theoretically not possible to determine a unique model from observations of apparent splitting parameters without independent constraints [e.g., *Hartog and Schwartz*, 2001].

[20] Thanks to the large number of high-quality measurements and the clear back azimuthal variations of ϕ and δt, we decided to search for the four best model parameters (ϕ lower layer, δt lower layer, ϕ upper layer, and δt upper layer) using the approach described by *Fontaine et al.* [2007]. Following the scheme described by *Silver and Savage* [1994] and for a dominant signal frequency of 0.1 Hz, we computed the apparent splitting back azimuthal variations for each two-layer model by varying in each layer the fast directions in steps of 2° (from 0°E to 180°E) and the delay time by steps of 0.2 s (from 0 to 2.6 s), providing a total of 1,353,690 models to test at each station. The fit between the observations and the theoretical apparent variations of the anisotropic parameters allows one to sort the models and to find the best fitting solutions characterized by the largest fitting parameter R^2_{adj} (adjusted standard misfit reduction) [*Walker et al.*, 2005; *Fontaine et al.*, 2007].

[21] Figures 4c and 4d present the observed splitting parameters together with the best two-layer model computed for station BKS. This best fitting model is characterized by an upper layer $\phi_1 = -30$°E and $\delta t_1 = 0.6$ s and a lower layer $\phi_2 = -78$°E and $\delta t_2 = 1.6$ s. This particular model slightly differs from the one proposed by *Ozalaybey and Savage* [1994] but falls within its uncertainties. It should be better constrained by the almost 15 years of supplementary recordings. The two-layer models were calculated for each station where consistent azimuthal variations where detected. In order to ensure that this methodology is not too influenced by the quality of the

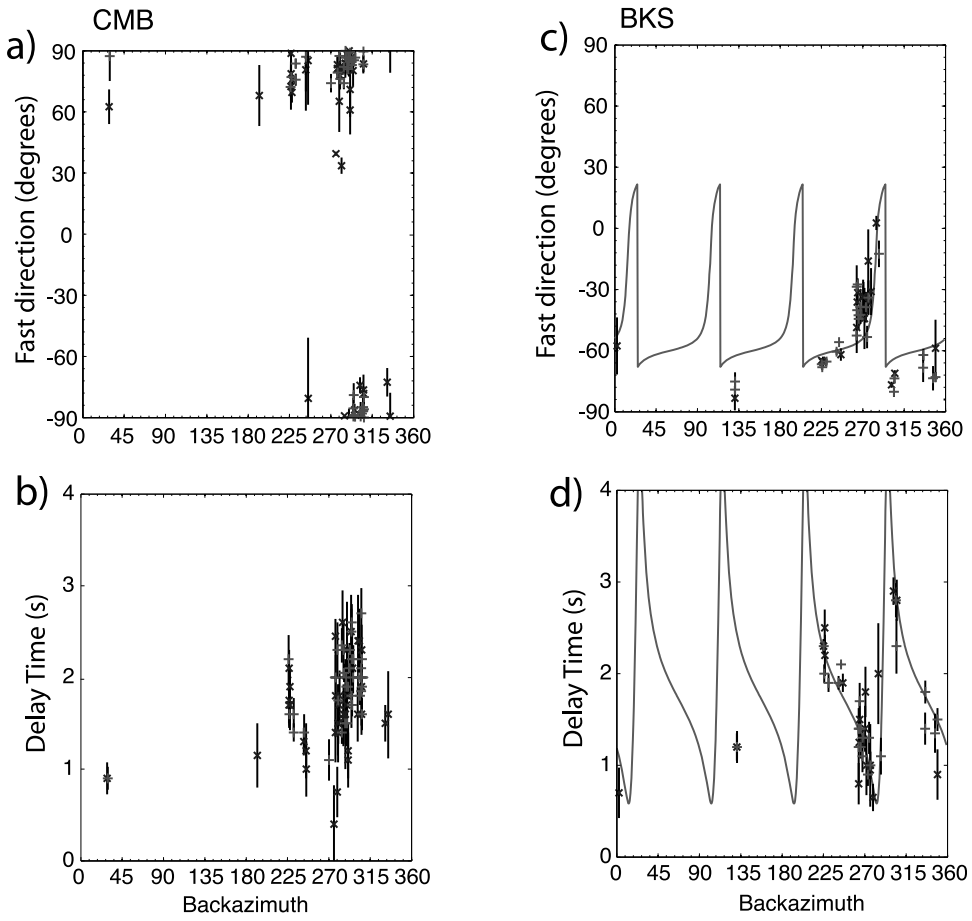

Figure 4. Individual splitting parameter values (ϕ, δt) with respect to event back azimuths. (a) Fast directions ϕ (in degrees) and (b) delay times δt (in seconds) obtained at station CMB (see location in Figure 1). (c) Fast directions and (d) delay times obtained at station BKS. The curves correspond to the best two-layer model: $\phi_1 = -30°$E, $\delta t_1 = 0.6$ s; $\phi_2 = -78°$E, $\delta t_2 = 1.6$ s. Errors bars correspond to the 95% confidence region.

splitting measurements, we systematically search for the best fitting two-layer model by using (1) all the splitting data, (2) only the good and fair splitting measurements, and (3) only good splitting measurements. Such an approach allows us to only keep models that have $R^2_{adj} > 0.5$, which indicates that at least 50% of the anisotropic signal can be explained by two layers of anisotropy.

[22] Figure 5 presents the results determined in this study at the stations where two-layer models provide a better solution than a single layer (see Table 3). These two maps clearly show that the stations requiring two anisotropic layers to explain the back azimuthal variations of the anisotropic parameters are clearly located close to the SAF system, as observed by *Ozalaybey and Savage* [1995] and *Hartog and Schwartz* [2001]. Our direct modeling concludes that the polarization directions within the upper layers (Figure 5a) show a good correlation with the strike of the main faults, whereas the orientation of the fast azimuths within the lower layers (Figure 5b) are more or less E–W, i.e., similar to the trend of the fast directions observed farther east.

3.4. Synthesis

[23] Figure 6 presents the final map of anisotropic parameters for central California. It includes all the (weighted) average splitting parameters for the stations with no back azimuthal variations, i.e., those underlain by a single anisotropic layer and the best two-layer models found at the other stations. The black dots represent stations without enough available data and where no reasonable average or double-layer model could be performed without including strong bias. These are mostly USArray stations that provided only 2 years of data and often produced a limited number of well-constrained splitting measurements.

[24] The map in Figure 6 shows a clear homogeneity of the fast polarization directions and delay times for most of the stations at which we did not find evidence of two anisotropic layers. We observe average ϕ values in the range N060°E to 90° and average δt close to 1.5 s. Interestingly, the E–W trending anisotropic directions are also detected on the western side of California beneath the SAF system for the deeper anisotropic layer, suggesting that such an anisotropic pattern could result from a single anisotropic structure and process, extending from the Pacific coast in the west to the Sierras in the east. These observations are indeed consistent with those of *Ozalaybey and Savage* [1995], *Hartog and Schwartz* [2000, 2001], and *Polet and Kanamori* [2002], which evidenced the existence of a regional layer beneath California, but also with large-scale

Table 2. Averaged Splitting Parameters Values for Stations Where No Back Azimuthal Variation Is Observed

Station	Latitude (deg)	Longitude (deg)	ϕ (deg)	δt (s)	Number of Measurements Averaged
CMB	38.035	−120.387	85 ± 1	1.8 ± 0.1	102
FARB	37.698	−123.000	−68 ± 3	1.9 ± 0.1	19
GASB	39.655	−122.716	−78 ± 18	0.9 ± 0.6	1
HAST	36.389	−121.551	−82 ± 4	1.4 ± 0.1	9
HELL	36.680	−119.023	−86 ± 9	1.2 ± 0.1	11
ISA	35.663	−118.474	88 ± 4	1.3 ± 0.1	10
KCC	37.324	−119.319	83 ± 2	1.5 ± 0.1	74
LAVA	38.755	−120.739	80 ± 3	1.1 ± 0.1	11
MIN	40.346	−121.607	49 ± 8	1.3 ± 0.4	3
MLAC	37.630	−118.836	58 ± 3	1.4 ± 0.1	14
O02C	40.177	−122.788	36 ± 9	1.6 ± 0.2	5
O04C	40.320	−121.086	68 ± 4	1.1 ± 0.1	11
O05C	39.962	−120.918	−87 ± 7	1.9 ± 0.3	8
ORV	39.555	−121.500	76 ± 5	1.1 ± 0.1	34
P01C	39.469	−123.338	−68 ± 6	1.5 ± 0.2	3
P05C	39.303	−120.608	61 ± 6	0.9 ± 0.2	6
R04C	38.257	−120.936	82 ± 3	1.5 ± 0.1	20
R05C	38.703	−120.076	62 ± 3	1.4 ± 0.1	12
R06C	38.523	−119.451	62 ± 4	1.5 ± 0.1	13
R07C	38.089	−119.047	51 ± 3	1.4 ± 0.1	11
RCT	36.305	−119.244	−81 ± 10	2.0 ± 0.5	1
S04C	37.505	−121.328	−80 ± 5	1.4 ± 0.2	11
S05C	37.346	−120.330	79 ± 3	1.55 ± 0.1	16
S06C	37.882	−119.849	67 ± 6	1.5 ± 0.1	7
S08C	37.499	−118.171	70 ± 3	1.5 ± 0.1	14
SAVY	37.389	−121.486	−81 ± 9	1.5 ± 0.1	7
SMM	35.314	−119.996	−67 ± 8	1.3 ± 0.1	11
SUTB	39.229	−121.786	−81 ± 9	1.1 ± 0.3	2
T06C	37.007	−119.709	85 ± 3	1.6 ± 0.1	19
TIN	37.054	−118.230	74 ± 2	1.8 ± 0.7	23
U05C	36.336	−120.121	−86 ± 8	1.5 ± 0.2	6
V03C	36.021	−121.236	86 ± 4	1.3 ± 0.1	9
V05C	35.867	−119.903	−86 ± 6	1.6 ± 0.3	4
VES	35.841	−119.085	−66 ± 10	1.2 ± 0.2	2

observations of upper mantle azimuthal anisotropy from surface wave tomography [e.g., *Debayle et al.*, 2005]. On the other hand, our findings show that the double-layer extent is geographically limited to the neighborhood of the SAF system, particularly in the south where results obtained at stations located at approximately 50 km from the fault do not show evidence of back azimuthal variations of the splitting parameters and therefore do not require two layers of anisotropy. Interestingly, close to the San Francisco Bay, the double anisotropic layer models seem to extend to a wider zone (about 100 km from the SAF in a strict sense), corresponding more or less to the extent of active faulting at the surface.

4. Discussion

4.1. Lateral Extent of the Anisotropy

[25] In section 3, we show that stations located on or close to the plate boundary are characterized by the presence of two anisotropic layers and that the upper anisotropic layer is likely related to plate boundary deformation (see Figure 6). By using individual splitting measurements instead of mean splitting values, we try in this section to provide more accurate evidence for the lateral extent of the plate boundary deformation. In order to approach the question of the location of the deformation at depth, and considering that the lithosphere thickness beneath western California is close to 70 km [e.g., *Melbourne and Helmberger*, 2001; *Li*, 2007], we project the splitting parameters along the seismic ray down to the 70 km depth piercing point (as schematically presented in Figure 7). Such an approach allows us to determine the distance d between the piercing point of the *SKS* ray at that depth and the surface trace of the fault and to study the relation between the anisotropy measurements and the surface trace of the faults. As shown in Figure 7 and assuming a vertical extent of the SAF throughout the lithosphere, a station installed

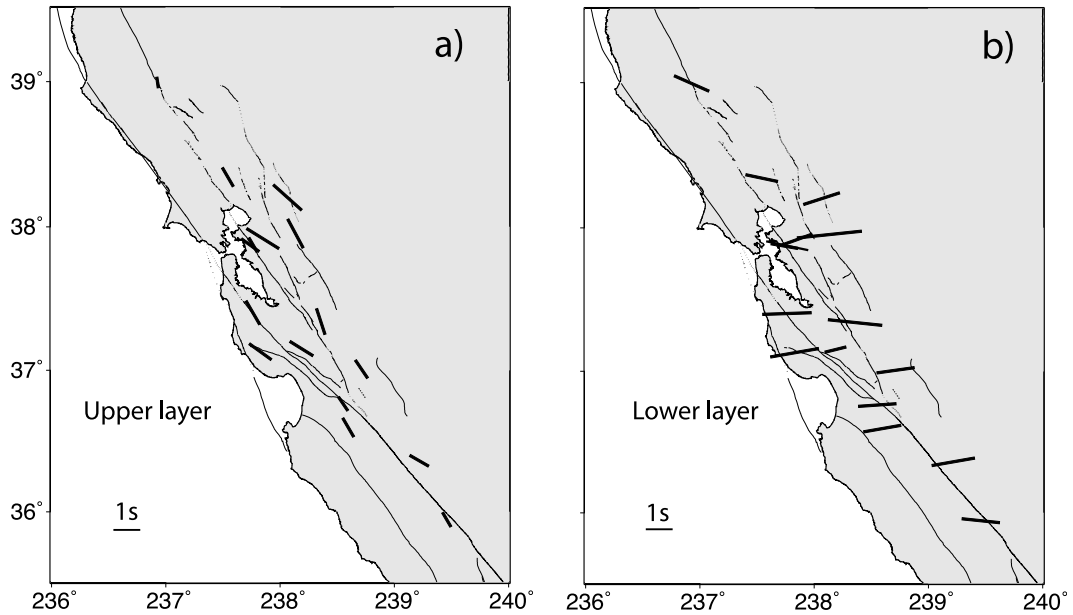

Figure 5. Anisotropic parameters of the best two-layer models obtained at stations where two layers are required to explain the *SKS* splitting: (a) upper layers and (b) lower layers.

Table 3. Splitting Parameter Values of the Best Two-Layer Models[a]

Station	Latitude (deg)	Longitude (deg)	ϕ_{up} (deg)	δt_{up} (s)	ϕ_{low} (deg)	δt_{low} (s)	R^2_{adj}
BDM	37.954	−121.866	−28	1.2	84	2.4	0.93
BKS	37.876	−122.236	−30	0.6	−78	1.6	0.73
BNLO	37.131	−122.172	−54	1.0	80	1.8	0.75
BRIB	37.919	−122.152	−58	1.4	70	1.2	0.84
BRK	37.874	−122.261	−54	0.8	−80	1.0	0.75
CVS	38.345	−122.458	−30	0.8	−78	1.6	0.5
FERN	37.153	−121.812	−58	1.0	76	0.8	0.81
HOPS	38.994	−123.072	−8	0.4	−66	1.4	0.54
JRSC	37.404	−122.239	−30	1.0	88	1.8	0.79
MHC	37.342	−121.643	−18	1.0	−84	2.0	0.8
PACP	37.008	−121.287	−34	0.8	82	1.4	0.73
PKD	35.945	−120.542	−30	0.6	−84	1.4	0.72
POTR	38.203	−121.935	−48	1.4	72	1.4	0.67
SAO	36.764	−121.447	−34	0.6	86	1.4	0.68
SCZ	36.598	−121.403	−30	0.8	80	1.4	0.88
U04C	36.363	−120.782	−60	0.8	80	1.6	0.63

[a] R^2_{adj} indicates the values of the correlation coefficient obtained between the models and the observations.

close to the fault itself may record *SKS* phases crossing an unperturbed mantle if the ray arrives from the east (*SKS* wave 1), and alternatively, a station installed east of the SAF may record seismic rays crossing the deep structure of the fault itself if the event arrives from the west (*SKS* wave 2). The width of the Fresnel zone obviously imposes a limit of resolution for that comparison. To go below that limit, one would need to apply finite-frequency techniques [e.g., *Favier and Chevrot*, 2003].

[26] Figure 8 presents the variations of splitting parameters ϕ and δt measured from individual events as a function of distance from the SAF in a strict sense (Figures 8a and 8b) or to the closest fault within the SAF system (Figure 8c). This allows us to estimate the lateral extent of the anisotropy at depth related to this fault, i.e., to locate the boundary between the region characterized by two anisotropic layers and the region characterized by a single anisotropic layer. The black curve corresponds to the variations of the mean splitting parameter for a 20 km wide moving window.

[27] In Figure 8a, average values of δt are globally constant and close to 1.5 s. A distance dependence is not apparent because of uncertainties of this parameter. The behavior of fast directions ϕ presented in Figure 8b appears to be rather different though: at large distance to the SAF fault (>100 km), the black curve is in the range 80° to 90° (consistent with the E–W Sierras directions), whereas close to the fault, the average is close to N120°E, illustrated by the large scatter observed in this region and explained by the strong back azimuthal variations related to the presence of two anisotropic layers. Figure 8b suggests that this two-layered domain extends relatively widely, between at least −50 (west) and 80 km (east) from the surface trace of the SAF. There is perhaps an asymmetry, which may possibly be due to the relative position of the San Andreas Fault within the plate boundary system, but it may also be due to the thinner lithosphere to the east the SAF [*Melbourne and Helmberger*, 2001]. The lithosphere might thus be more deformable there than on the western side, leading to strain and formation of anisotropy preferentially in the eastern part.

[28] In order to take into account not only the deformation induced by the SAF itself but also the other faults that may together accommodate the strike-slip deformation at depth (Calaveras, Hayward, Greenville faults, etc.), Figure 8c shows the variations of ϕ with respect to the distance to the closest fault (and not specifically the SAF in a strict sense). The pattern is different in the sense that the scattered values are now grouped more closely to 0 km. The average curve decays more quickly with distance, suggesting not only that the San Andreas Fault is a source of anisotropy at depth but that the other strike-slip faults of the system also produce back azimuthal variations of the anisotropic parameters and hence two anisotropic layers. This implies that those other faults are likely lithospheric faults and not restricted to the crust. This analysis provides a simple (but certainly oversimplified) view of the plate boundary that consists of a set of faults, each extending throughout the entire lithosphere and that each of these faults is about 40 km wide in the lithospheric mantle. At this level of

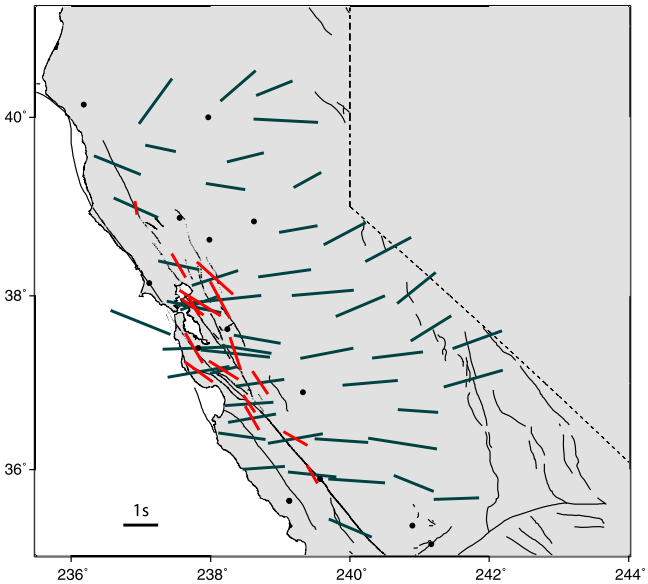

Figure 6. Anisotropy map of central California presenting the averaged splitting measurements together with the best two-layer models. Red bars are upper layers of the two-layer models. Black dots indicate stations where neither averaging nor two-layer modeling could be performed.

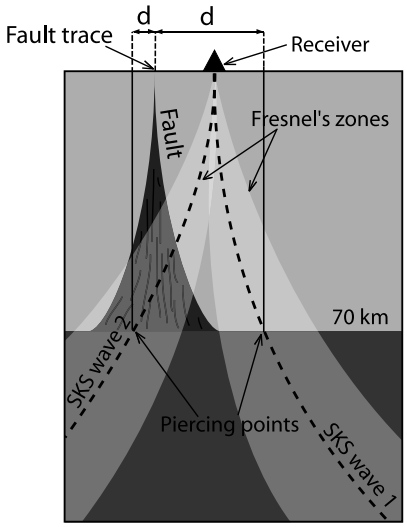

Figure 7. Cartoon explaining the way the individual splitting measurements are projected in Figure 8 in order to evaluate the actual distance between the fault and the 70 km (i.e., the assumed bottom of the lithosphere) depth piercing point. Horizontal distance between the 70 km piercing point of the *SKS* wave to the surface trace of the fault(s) is represented by *d*. Note that for a station close to the fault, *SKS* waves may sample the upper mantle from each side of the fault depending on the wave back azimuth. The shaded area illustrates the width of the Fresnel zone for each *SKS* wave, calculated for a dominant period of 10 s.

inference, the deformation appears to be more or less symmetric across the faults, and the entire SAF system appears to be about 130 km wide (Figure 8c). One has, however, to notice that these observations do not take into account the width of the Fresnel zone of the *SKS* waves at 70 km depth (close to 100 km). The proposed width of the deformation zone associated with strike-slip faults in California is therefore a minimum value.

4.2. Vertical Location and Extent of the Anisotropy

[29] The major limitation in interpreting *SKS* splitting is that there is no direct constraint on the vertical location of the anisotropy. Theoretically, because *SKS* waves are generated at the core-mantle boundary, the splitting could be acquired everywhere along its 2900 km long path to the Earth's surface. There is, however, a large consensus concerning the overall isotropy of the lower mantle [e.g., *Meade et al.*, 1995] although seismic anisotropy has been described in its lowermost part in the D″ region for horizontally propagating *S* waves [e.g., *Kendall and Silver*, 1998] and although anisotropy may be also locally present beneath the transition zone in some subduction environments [e.g., *Wookey et al.*, 2002]. Petrophysical investigation of the transition zone suggests that it may be weakly anisotropic due to the small intrinsic anisotropies of the constituting mineral phases [e.g., *Mainprice et al.*, 2000; *Mainprice et al.*, 2008]. The analysis of olivine slip systems at upper mantle depths finally suggests that most preferred orientations are likely concentrated in the uppermost 300 km of the Earth [*Mainprice et al.*, 2005], which is confirmed by the systematic presence of olivine lattice-preferred orientation in natural peridotites, like basalt xenoliths [e.g., *Pera et al.*, 2003], kimberlite nodules [e.g., *Ben Ismail et al.*, 2001], orogenic peridotite bodies [e.g., *Peselnick et al.*, 1974], or ophiolite massifs [e.g., *Jousselin and Mainprice*, 1998]. From a seismological point of view, analyses of the sensitivity kernels suggest that the *SKS* waves are primarily sensitive to anisotropy in the uppermost 300 to 400 km of the Earth [*Sieminski et al.*, 2007], i.e., in the uppermost lithospheric and asthenospheric mantle. This is consistent with the large-scale global correlation between the anisotropy patterns derived from surface waves [e.g., *Debayle et al.*, 2005] and *SKS* splitting observations [*Wüstefeld et al.*, 2009].

[30] In this section we discuss the vertical location of the deformation by taking into account the observed delay times, the possible thicknesses of the various anisotropic layers, and the possible intrinsic magnitude of anisotropy that could be constrained independently through petrophysical analyses of mantle rocks. Such discussion has to take into account the geological settings (lithosphere thickness, locations, and orientations of the geologic structures).

4.2.1. Regional, "E–W" Anisotropy

[31] This work presents evidence for a regional anisotropic layer beneath the entire study area that is characterized by a N060°E to E–W fast directions and by high and constant delay times around 1.5 s (see Figure 6). Considering that the lithosphere beneath central California is only 70 km thick [e.g., *Melbourne and Helmberger*, 2001; *Li*, 2007], including a crustal thickness of 25 km close to the SAF and 50 km beneath the Sierras [e.g., *Mooney and Weaver*, 1989], one has to admit that the anisotropic signal is likely acquired in the sublithospheric mantle, i.e., within the asthenosphere.

[32] In the Sierras, where the crust is relatively thick, the only 20 km thick mantle lid of the lithosphere is likely not thick enough to explain the 1.5 s observed delay times in terms of lithospheric deformation alone. Petrophysical data indeed suggest that the crust is able to produce maximum delay times in the range of 0.1 to 0.2 s per 10 km of path, depending on the overall mineralogy, fabric strengths, and orientations [*Barruol and Mainprice*, 1993b]. One could therefore expect a maximum of 0.5 s of crustal delay time, still requiring at least 1.0 s supplementary splitting to be explained within the upper mantle. The presence of such large amounts of anisotropic signal in the crust is, however, unlikely since seismological measurements of the whole crustal shear wave splitting, using Moho *Ps* converted phases in the neighboring Basin and Range [*McNamara and Owens*, 1993], have shown a total crustal delay time around 0.2 s, implying an upper mantle delay time of about 1.3 s that would require very high intrinsic anisotropy to be located in the 20 to 45 km thick lithospheric mantle lid.

[33] Typical values of anisotropy magnitudes of upper mantle rocks are in the range of 4% to 5% for shear waves propagating parallel to the *Y* structural direction, i.e., normal to the lineation within the foliation, and in the range of 2% to 3% for waves propagating along the *Z* structural direction, i.e., normal to the foliation [*Mainprice and Silver*, 1993; *Ben Ismail and Mainprice*, 1998; *Mainprice*, 2000]. Taking into account that the foliation within the asthenosphere deformed by the overlying plate drag is expected to be horizontal and that the *SKS* waves propagate along the

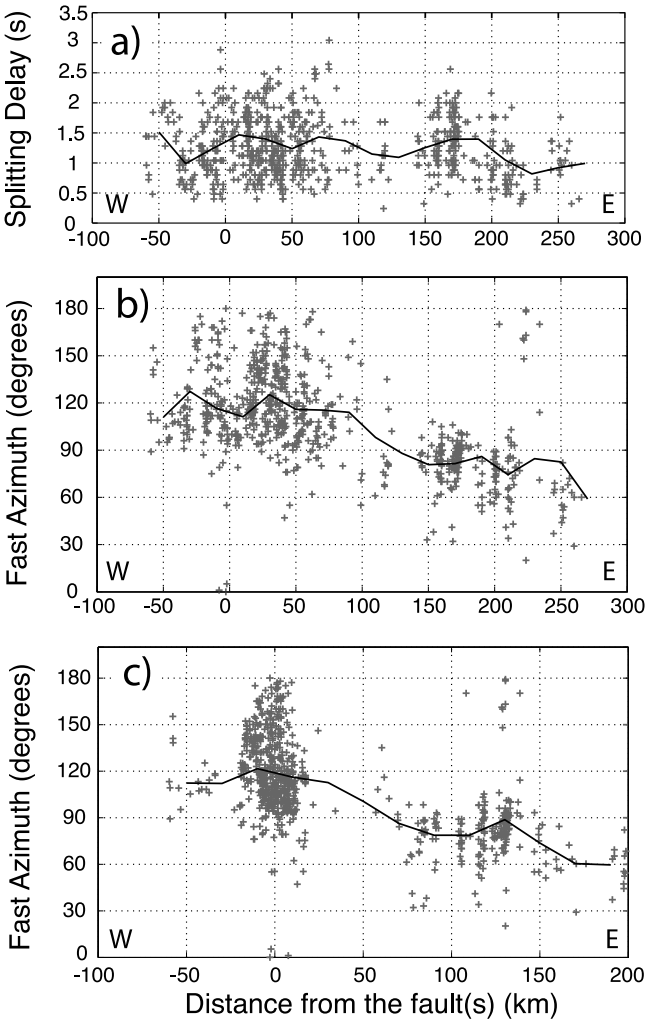

Figure 8. Diagram of the splitting parameter values with respect to distance d to the faults (as defined in Figure 7). (a) Delay times and (b) fast directions, with distance from the San Andreas Fault in a strict sense. (c) Fast directions as a function of distance from the closest fault within the SAF system.

vertical direction, i.e., normal to the foliation, we deduce from the relation $L = (\delta t V_s)/A$, linking delay time δt, velocity of the shear wave considered (here SKS) V_s, anisotropy magnitude A, and length of the anisotropic path L (Figure 9), that the thickness of the regional anisotropic layer may explain that the observed regional delay times must be in the range 150 to 250 km.

[34] Obviously, the absence of stronger constraints on the anisotropy magnitude allows envisaging various alternatives. Anisotropy magnitudes smaller than 4% ($A < 0.04$) will require a longer anisotropic path to explain the 1.5 s of delay time (for instance, about 300 km for 2% anisotropy), but alternatively, stronger anisotropy should result in a thinner anisotropic layer. For instance, *Ozalaybey and Savage* [1995] proposed stronger values of S wave anisotropy (8%) in order to explain all the splitting by lithospheric anisotropy. However, studies of xenoliths of lithospheric origin sampled close to the SAF [*Titus et al.*, 2007] or in the Mojave Desert in southern California [*Soedjatmiko and Christensen*, 2000] indicate 4% to 5% of maximum anisotropy for shear waves and therefore do not favor such a hypothesis. All the arguments above converge to the conclusion that the lithosphere in the eastern part of California can hardly explain the whole anisotropic signal. This is also confirmed by other geophysical observables, such as global surface wave tomographic models [e.g., *Debayle et al.*, 2005] that show clear E–W trending fast direction beneath the western United States at a depth between 150 (if 5% anisotropy magnitude) and 250 km (if 3% anisotropy magnitude), favoring an asthenospheric location for the E–W trending anisotropic layer.

4.2.2. San Andreas Fault System

[35] In the SAF area, we have shown that anisotropy is characterized by a two-layer structure. The deeper layer clearly has the same characteristics as the regional anisotropy discussed in section 4.2.1 and is probably located in the asthenosphere as a 150 to 250 km thick deformed layer. This section will thus focus on the upper layer that we relate to the deformation of the plate boundary, partly because of the parallelism of ϕ with the trend of the faults.

[36] This upper layer is characterized by delay times generally smaller than 1.0 s, with an average around 0.7 s. Such delay times may result from a relatively thin anisotropic layer in the range 50 to 100 km thick (Figure 9), which is consistent with the lithospheric thickness in this area (<70 km thick), especially to the east of the SAF [e.g., *Melbourne and Helmberger*, 2001; *Li*, 2007], including a 25 km thick crust [e.g., *Mooney and Weaver*, 1989]. Contrary to the Sierras, this region is crosscut by numerous vertical strike-slip faults that may have produced pervasive vertical foliations and horizontal lineations in the middle and the lower crust, which is the most efficient orientation of the pervasive structures relative to the vertically propagating *SKS* waves to generate high δt. In such geometry, delay times of 0.1 to 0.2 s per tens of kilometers of strained crust could be therefore produced [*Barruol and Mainprice*, 1993b] and may reasonably explain 0.2 to 0.4 s. Aligned microcracks in the uppermost crust can also potentially produce anisotropy and therefore shear wave splitting. However, studies at San Andreas Fault Observatory at Depth (SAFOD) site, near Parkfield, showed from local seismicity that crack-induced delays are smaller than 0.1 s for 15 km long raypaths [e.g., *Liu et al.*, 1997; *Liu et al.*, 2008] and that crack-induced fast polarization directions in the vicinity of the fault are trending N010°E, i.e., parallel to the maximum horizontal stress in California and thus at a large angle to the fault. Although their signature is likely, upper and lower crustal anisotropies are therefore too low to explain the entire observed delay times close to the SAF but can possibly produce 0.2 to 0.4 s of splitting delay, i.e., approximately 50% of the observed upper layer anisotropic signal. This is of interest in light of the debate over the last years as to whether the faults are merely crustal features [e.g., *Brocher et al.*, 1994; *Parsons and Hart*, 1999].

[37] The upper mantle anisotropy beneath the SAF can be locally constrained by direct peridotite sampling brought up at the Earth's surface by recent volcanism. *Titus et al.* [2007] showed, by studying xenoliths sampled near the SAF between Parkfield and San Francisco, that a rather strong fabric (inducing 5% of S wave anisotropy) is present

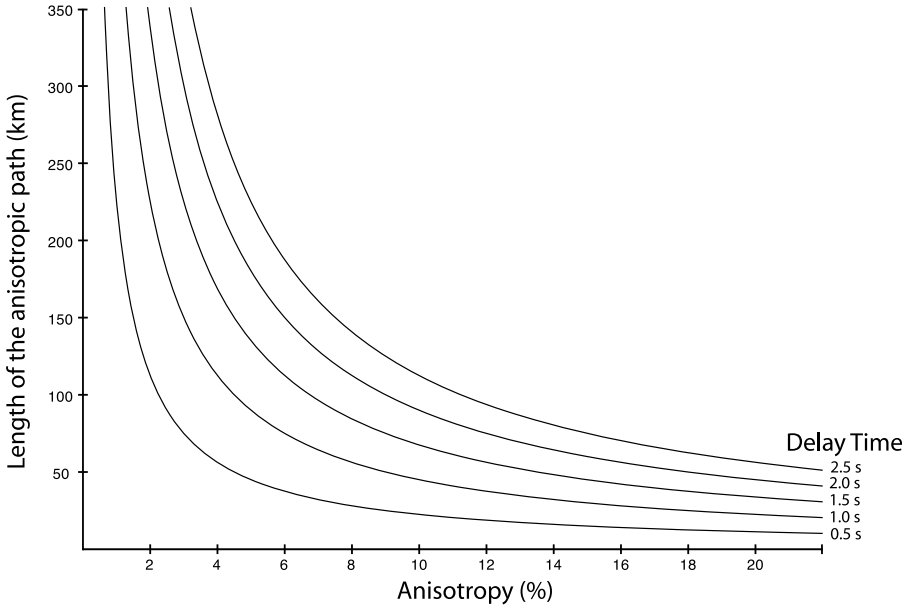

Figure 9. Thickness (L) of the anisotropic layer crossed by *SKS* waves with respect to anisotropy magnitude (A) for various delay time (δt). $L = (\delta t V_s)/A$. On the horizontal axis, "Anisotropy" corresponds to $A \times 100$.

at lithospheric mantle depth beneath the SAF. Such anisotropy magnitude suggests that the missing 0.5 s of delay time can be easily acquired in a 50 km thick lithospheric mantle (Figure 9). The lithosphere beneath the SAF system is therefore sufficient to explain the entire delay time corresponding to the upper layer at the various two-layer stations. Interestingly, in the case of a strike-slip fault, both the crustal and upper mantle layer will add their effect together and will be seen as a single anisotropic layer. In the crust, foliations are expected to be steeply dipping and parallel to the fault, and the lineations are expected to be horizontal, providing fast split shear waves parallel to the fault, whereas in the mantle, such a system should align the olivine *a* axes horizontal and parallel to the fault [e.g., *Tommasi et al.*, 1999], also producing fast split shear waves parallel to the fault. Seismic waves crossing this area along a vertical path should therefore see the lithospheric mantle and the overlying crust as a single anisotropic layer.

[38] Interestingly, independent seismological observations in the western United States provide similar conclusions on the fault-related lithospheric anisotropy. Azimuthal velocity variations of *Pn* waves that propagate horizontally beneath the Moho show a NW–SE fast trend beneath central western California, compatible with the strike of the main Californian faults [*Hearn*, 1996]. This study indicates (1) that there is no E–W trending anisotropic layer that affects the upper part of the lithosphere and (2) that the SAF-related anisotropy is likely concentrated in the vicinity of the fault, as we show from the *SKS* splitting. Azimuthal anisotropy deduced from regional surface waves tomography from ambient noise correlation [*Lin et al.*, 2009] also clearly indicates fast polarization directions correlated with the faults strike at periods of 24 s and also at periods of 12 s, indicating a possible coherence of anisotropy between the crust and the uppermost lithospheric mantle. *Lin et al*. [2009] also constrain the lateral extent of this fault-parallel fast direction from the Pacific coast to the western border of the Great Valley, compatible with the deformation broadness evidenced by our *SKS* measurements.

4.3. Geodynamic Interpretation

4.3.1. SAF System Anisotropic Layer

[39] As mentioned in section 4.2.2, in the case of large-scale strike-slip faults, the associated strain likely extends from the ductile crust down to the lithospheric mantle. The accommodation of the deformation may develop pervasive structures such as vertical foliation and horizontal lineation parallel to the fault strike. The modest scatter of the fast directions in the upper layer, and the good fit with the faults orientations, agree with such structures. Such a strike-slip tectonic regime is ideal to produce strong *SKS* splitting response [*Tommasi et al.*, 1999] and agrees with the fact that a thin lithosphere, even with little mantle lithosphere (as observed here), can be sufficient to explain our observations, i.e., 0.5 to 1.0 s of splitting delays (see Figure 9). Those observations favor a deep extent of the SAF system, i.e., across the whole lithosphere, and thus bring important information in the debate on the possible mantle extension of the San Andreas Fault [*Brocher et al.*, 1994; *Teyssier and Tikoff*, 1998; *Parsons and Hart*, 1999]. The poor vertical resolution of the *SKS* waves does not allow constraining the existence of a decoupling zone at the base of the upper crust [*Bokelmann and Beroza*, 2000]. Another interesting observation is the northward decay of the splitting delay toward the Mendocino Triple Junction, which is coherent with the plate boundary related deformation, since the strain is expected to go to zero at the triple junction; the relation

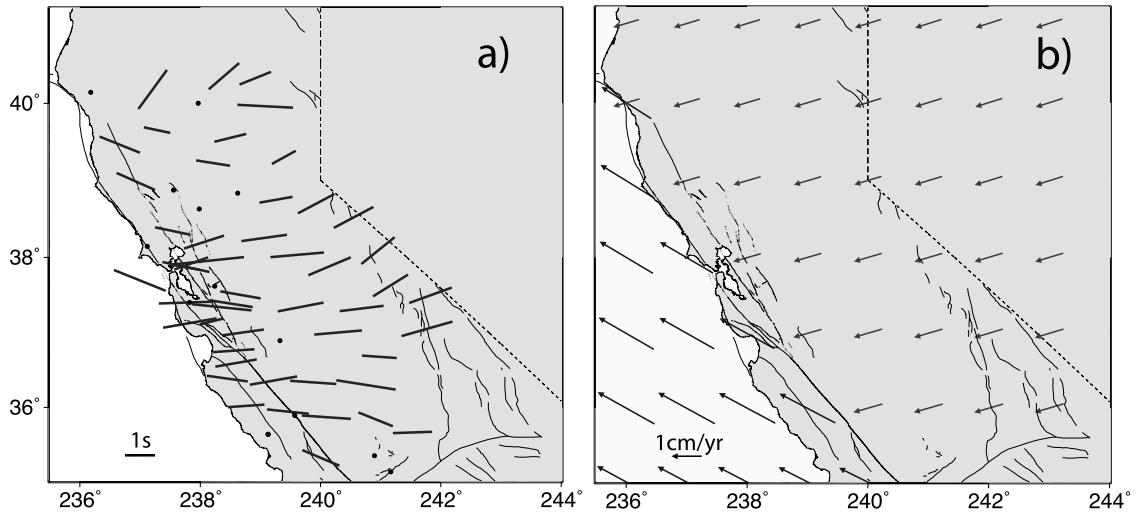

Figure 10. (a) Splitting measurements for single-layer stations, as well as the lower layer from two-layer stations. (b) Absolute plate motion (APM) in HS3_NUVEL-1A reference frame [*Gripp and Gordon*, 2002] of the Pacific and North American plates.

between latitude and delay time, however, is not clear for the southern and central stations.

4.3.2. Absolute Plate Motion Versus Seismic Fast Orientations

[40] We have evidenced an E–W to NW–SE rotation of fast direction from the east to the west of what we interpret as asthenospheric deformation (Figure 6). A possible explanation may lie in the absolute plate motion (APM) of the North American and Pacific plates, e.g., in the differential movements between the lithosphere and the underlying mantle that may produce large strain [*Silver*, 1996; *Savage*, 1999]. *Hartog and Schwartz* [2001] already noticed the good correlation between APM directions and anisotropic fast polarizations but only for North American parameters, as they did not process measurements on the Pacific plate.

[41] Figure 10a presents the splitting related to the lower layer, as well as that of the single-layer stations, and compares them with the APM vectors calculated in the HS3-NUVEL-1A reference frame [*Gripp and Gordon*, 2002] for the Pacific and North American plates (Figure 10b). Interestingly, the APM directions correlate well with the overall observed fast split directions far from the SAF for both the eastern domains, where ϕ trends close to E–W (close to the North American APM), and to the west of the SAF with a NW–SE trending ϕ (close to the Pacific APM), mainly documented by station FARB (see Figure 1a for location). This agreement across the plate boundary at large scale may therefore confirm the notion of plate motion related anisotropy in the asthenospheric layer. We note, however, that the transition between the two regions is much smoother in the splitting observations than in the APM vectors.

[42] In an APM-related anisotropy model, the North American plate that goes westward should progressively move over an asthenospheric mantle that was previously beneath the Pacific plate (Figure 11). The normal component of North America according to the plate boundary is about 1 cm/yr and similar in amplitude to the normal component of the Pacific motion (Figures 11a and 11b). The American plate thus covers old Pacific mantle at the rate of 10 km/Myr. The type of deformation remains nearly simple shear, but the direction of strain changes with time and location. We may thus expect that Pacific fast directions (NW–SE) are gradually replaced by E–W fast directions thus forming a smooth transition area (Figures 11c and 11d). The plate boundary represents the western limit of the region where the transition takes place. Although the number of measurements on the Pacific plate itself is small, this mechanism may thus explain the observed asymmetry rather naturally. This model also implies that "North American" E–W fast directions can never be observed to the west of the western limit of the plate boundary (the San Gregorio Fault, etc.).

[43] We have observed in Figure 8 that the rotation appears to be complete about 140 km to the east of the San Andreas Fault, i.e., 14 Myr after the San Andreas Fault has passed over the deeper mantle in that region. Interestingly, that distance roughly corresponds to the vertical thickness of the zone over which the deformation probably occurs within the asthenosphere.

[44] An alternative way to explain a rotation of deep anisotropy across California is to invoke an eastward oriented mantle flow [*Silver and Holt*, 2002]. Such a view is coherent with large-scale mantle dynamics under the North American plate [e.g., *Bokelmann*, 2002], and explains the anistropy observations in central California. However, the observations are more easily explained by the motion of the plate boundary itself.

4.3.3. Other Geodynamic Models

[45] Besides the simple mantle replacement model that we presented in section 4.3.2, there are further geodynamic elements in California that may be addressed using seismic anisotropy. In our region of interest, the Farallon plate and its remnants have been subducting nearly E–W beneath North America [*Severinghaus and Atwater*, 1990] and thus possibly produced an E–W trending flow within the North American mantle that would be in agreement with the fast observed directions. Subduction of the East Pacific Rise at 29 Ma [*Atwater*, 1970] provoked the detachment of the flat

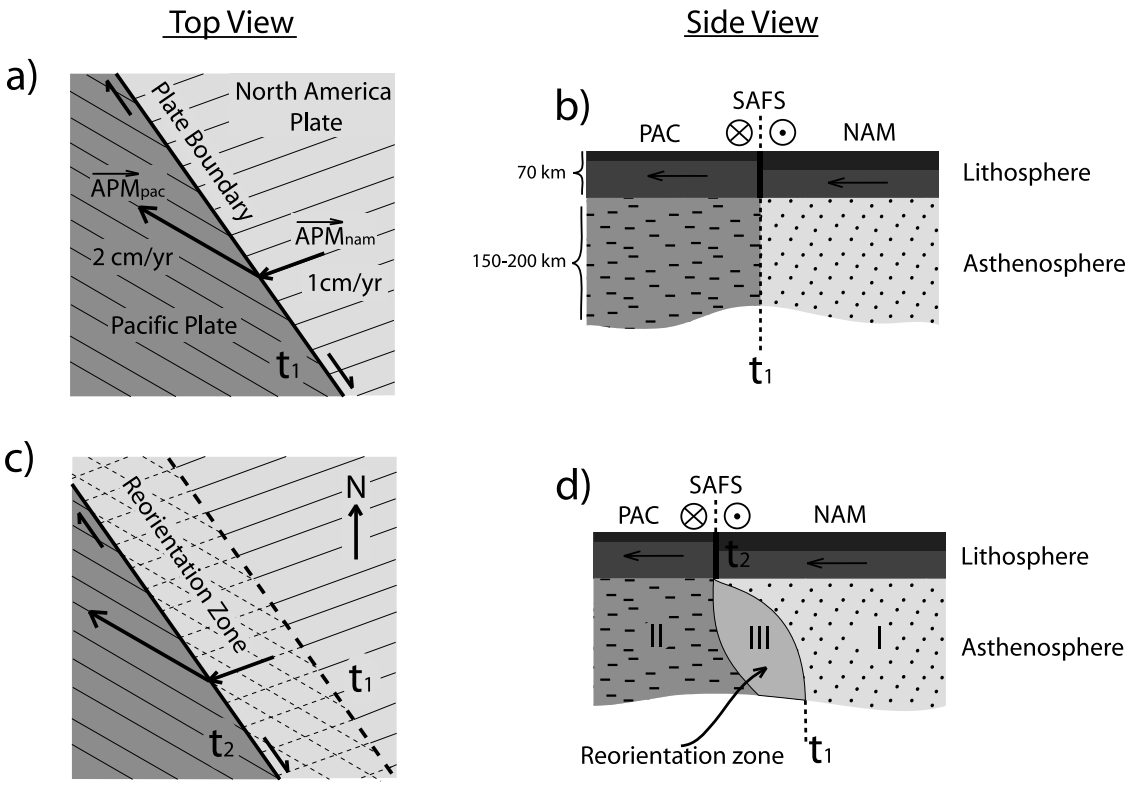

Figure 11. Cartoons illustrating the Pacific and North American plate motions. The plate boundary is shown (a) at time t_1 and (c) at time t_2. (b and d) Cross sections which show how the plate boundary (and part of the North American plate) is moving over mantle that was previously beneath the Pacific plate. In Figure 11d, areas I, lineation parallel to the APM of the North American plate; II, lineation parallel to the APM of the Pacific plate at asthenospheric depth; and III, intermediate directions of lineation.

Farallon slab [*Coney and Reynolds*, 1977; *Humphreys*, 2008], opening a slab-free window beneath western North America [*Dickinson and Snyder*, 1979]. The asthenospheric flow that filled the gap left by the slab has indeed been evoked previously to explain the E–W anisotropic trend [*Ozalaybey and Savage*, 1995; *Hartog and Schwartz*, 2001] but does not explain the smooth rotation of the fast directions observed in central California. On the other hand, the three northernmost stations of our study (O02C, O04C, and MIN) located, as shown by seismic tomography [*Van der Lee and Nolet*, 1997; *Burdick et al.*, 2008], above the Juan de Fuca slab that is a remnant of the Farallon plate, show fast directions in the range N35°E to N50°E that is close to the N15°E to N25°E trend of the Juan de Fuca APM [*Gripp and Gordon*, 2002]. As previously suggested by *Bostock and Cassidy* [1995] for the station close to Vancouver, fast directions from *SKS* splitting probably indicate that anisotropy in this area is related to the corner flow above the slab.

4.3.4. Synthesis

[46] Figure 12 is a cartoon that summarizes our observations pertaining to the Californian plate boundary, including the different anisotropic layers and their vertical extent, the possible orientation of the pervasive structure (foliation and lineation), and some other tectonic features, such as the lithosphere thicknesses. Our observations allow us to propose that the anisotropic layer associated with the SAF system is a 50 to 80 km thick deformed structure localized within the lithosphere and characterized by a vertical foliation with a fault-strike parallel lineation. At lower lithospheric depths, this zone does not extend laterally more than 100 to 150 km from the surface strike of the SAF (in a strict sense) in zones where deformation is distributed. This fault-related anisotropy is overlying and decoupled from a regional (asthenospheric) layer that is likely 150 to 250 km thick, probably with a horizontal foliation and, as explained in Figure 11, with lineation parallel to the North American APM directions beneath the Sierra Nevada (area I) to Pacific APM directions west from the Californian coast (area II), with a smooth transition beneath the plate boundary where intermediate directions are observed (area III). However, even if this model is attractive for explaining our observations, the other tectonic processes, such as the Farallon subduction and the propagation of the slab-free window, may also generate lineations in the upper mantle close to E–W strikes and therefore may superimpose their own signatures with the APM-induced deformation.

5. Conclusion

[47] The analysis of shear wave splitting performed at 65 broadband stations in central California allowed us to investigate upper mantle deformation beneath California and especially across the strike-slip plate boundary between the North American and the Pacific plates. The large number of permanent and temporary seismic stations permits us to

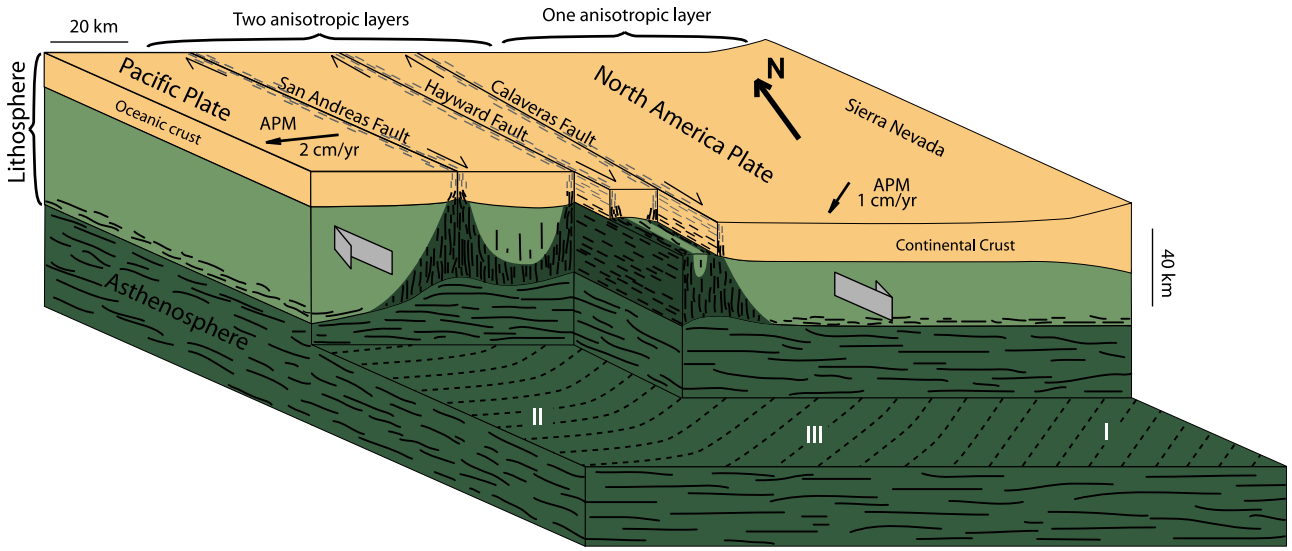

Figure 12. Block diagram summarizing the lithospheric and asthenospheric structures beneath northern California. Areas I, lineation parallel to the APM of the North American plate within the deforming asthenosphere; II, lineation parallel to the APM of the Pacific plate; and III, intermediate directions of lineation corresponding to the reorientation zone.

discuss the horizontal and vertical extent of the upper mantle deformation from the Sierra Nevada to the Californian coasts.

[48] Our analysis reveals two different anisotropic domains: (1) a zone extending from the Sierra Nevada to the Great Valley where splitting measurements require a single, E–W trending anisotropic layer and (2) the SAF system region where two anisotropic layers are required, an upper layer trending parallel to the fault overlying an E–W trending lower layer. The E–W regional fast directions likely correspond to a 150 to 250 km thick asthenospheric layer deformed by the relative motion between the North American plate and the underlying mantle. In the plate boundary region, the upper of the two layers is clearly associated with the dynamics of the SAF system (fast anisotropic directions close to the faults' strikes) and suggests that the whole lithosphere (i.e., the crust and the lithospheric mantle) deforms coherently and is thus decoupled from sublithospheric flow. Thanks to the good seismic coverage and the large amount of data, we estimated the lateral extent of the deformation zone associated with the SAF system. We propose that around each single strike-slip fault, the lithospheric mantle deformation is concentrated in a 40 km broad strip, providing a total broadness of deformed San Andreas Fault zone to be around 130 km at lower lithospheric levels. The good fit between APM of the North American plate and the fast anisotropic directions leads us to suggest that shear produced by the relative motion of the lithosphere overlying the asthenosphere is a good candidate for the origin of this layer. The motion of the plate boundary and the North American lithosphere over an old Pacific mantle with NW–SE fast directions can also be invoked to explain the smooth transition of the fast directions from the east to the west. The lower layer could be thus characterized by a horizontal foliation with lineation parallel to the absolute plate motion of the North American plate in the east and with lineation parallel to the Pacific APM in westernmost California. The relatively large thickness of this asthenospheric layer (150 to 250 km) is also coherent with the presence of a slab-free window beneath the western United States that entrained hot and therefore softened material close to the lithosphere-asthenosphere boundary that could be more easily deformed. In a different way, the fast directions observed for the northernmost stations, localized north of the Mendocino Triple Junction, are close to the APM direction of the Juan de Fuca plate and thus can be interpreted as the signal of the Juan de Fuca slab subducting beneath North America.

[49] **Acknowledgments.** The facilities of the IRIS Data Management System and, specifically, the IRIS Data Management Center, were used for access to waveform and metadata required in this study. The IRIS DMS is funded through the National Science Foundation and, specifically, the GEO Directorate through the Instrumentation and Facilities Program of the National Science Foundation under Cooperative Agreement EAR-0004370. Thanks to Geoscope, to Berkeley, and to the Southern California Seismic Network, operated by Caltech and USGS, for the availability and the high quality of the data. Data from the Transportable Array (TA) network were made freely available as part of the EarthScope USArray facility supported by the National Science Foundation, Major Research Facility program under Cooperative Agreement EAR-0350030. We thank the two anonymous reviewers for the constructive comments that improved the manuscript. SplitLab software and the *SKS* splitting database are available at http://www.gm.univ-montp2.fr/splitting/.

References

Atwater, T. (1970), Implications of plate tectonics for the Cenozoic tectonic evolution of the western North America, *Geol. Soc. Am. Bull.*, *81*, 3513–3536, doi:10.1130/0016-7606(1970)81[3513:IOPTFT]2.0.CO;2.

Barruol, G., and R. Hoffmann (1999), Seismic anisotropy beneath the Geoscope stations from *SKS* splitting, *J. Geophys. Res.*, *104*, 10,757–10,774, doi:10.1029/1999JB900033.

Barruol, G., and D. Mainprice (1993a), 3D seismic velocities calculated from LPOs and reflectivity of a lower crustal section: Example of the Val Sesia (Ivrea Zone, northern Italy), *Geophys. J. Int.*, *115*, 1169–1188, doi:10.1111/j.1365-246X.1993.tb01519.x.

Barruol, G., and D. Mainprice (1993b), A quantitative evaluation of the contribution of crustal rocks to the shear wave splitting of teleseismic *SKS* waves, *Phys. Earth Planet. Inter.*, *78*, 281–300, doi:10.1016/0031-9201(93)90161-2.

Ben Ismail, W., and D. Mainprice (1998), An olivine fabric database: An overview of upper mantle fabrics and seismic anisotropy, *Tectonophysics*, *296*, 145–157, doi:10.1016/S0040-1951(98)00141-3.

Ben Ismail, W., G. Barruol, and D. Mainprice (2001), The Kaapvaal craton seismic anisotropy: Petrophysical analyses of upper mantle kimberlite nodules, *Geophys. Res. Lett.*, *28*, 2497–2500, doi:10.1029/2000GL012419.

Bokelmann, G. H. R. (2002), Which forces drive North America?, *Geology*, *30*, 1027–1030, doi:10.1130/0091-7613(2002)030<1027:WFDNA>2.0.CO;2.

Bokelmann, G. H. R., and G. C. Beroza (2000), Depth-dependent earthquake focal mechanism orientation: Evidence for a weak zone in the lower crust, *J. Geophys. Res.*, *105*, 21,683–21,696, doi:10.1029/2000JB900205.

Bokelmann, G. H. R., and R. L. Kovach (Eds.) (2000), *Proceedings of the 3rd Conference on the Tectonic Problems of the San Andreas Fault System*, 384 pp., Stanford Univ., Stanford, Calif.

Bostock, M. G., and J. F. Cassidy (1995), Variations in *SKS* splitting across western Canada, *Geophys. Res. Lett.*, *22*, 5–8, doi:10.1029/94GL02789.

Bowman, J. R., and M. Ando (1987), Shear-wave splitting in the upper-mantle wedge above the Tonga subduction zone, *Geophys. J. R. Astron. Soc.*, *88*, 25–41.

Brocher, T. M., J. McCarthy, P. E. Hart, W. S. Holbrook, K. P. Furlong, T. V. McEvilly, J. A. Hole, and S. L. Klemperer (1994), Seismic evidence for a lower-crustal detachment beneath San Francisco Bay, California, *Science*, *265*, 1436–1439, doi:10.1126/science.265.5177.1436.

Burdick, S., C. Li, V. Martynov, T. Cox, J. Eakins, T. Mulder, L. Astiz, F. L. Vernon, G. L. Pavlis, and R. D. van der Hilst (2008), Upper mantle heterogeneity beneath North America from travel time tomography with global and USArray Transportable Array data, *Seismol. Res. Lett.*, *79*(3), 384–392, doi:10.1785/gssrl.79.3.384.

Coney, P. J., and S. J. Reynolds (1977), Flattening of the Farallon slab, *Nature*, *270*, 403–406, doi:10.1038/270403a0.

Crampin, S. (1984), Effective anisotropic elastic constants for wave propagation through cracked solids, *Geophys. J. R. Astron. Soc.*, *76*, 135–145.

Debayle, E., B. L. N. Kennett, and K. Priestley (2005), Global azimuthal seismic anisotropy and the unique plate-motion deformation of Australia, *Nature*, *433*, 509–512, doi:10.1038/nature03247.

Dickinson, W. R., and W. S. Snyder (1979), Geometry of the subducted slabs related to the San Andreas transform, *J. Geol.*, *87*, 609–627, doi:10.1086/628456.

Favier, N., and S. Chevrot (2003), Sensitivity kernels for shear wave splitting in transverse isotropic media, *Geophys. J. Int.*, *153*, 213–228, doi:10.1046/j.1365-246X.2003.01894.x.

Fontaine, F. R., G. Barruol, A. Tommasi, and G. H. R. Bokelmann (2007), Upper mantle flow beneath French Polynesia from shear-wave splitting, *Geophys. J. Int.*, *170*, 1262–1288, doi:10.1111/j.1365-246X.2007.03475.x.

Gripp, A. E., and R. B. Gordon (2002), Young tracks of hotspots and current plate velocities, *Geophys. J. Int.*, *150*, 321–361, doi:10.1046/j.1365-246X.2002.01627.x.

Hartog, R., and S. Schwartz (2000), Subduction-induced strain in the upper mantle east of the Mendocino Triple Junction, California, *J. Geophys. Res.*, *105*, 7909–7930, doi:10.1029/1999JB900422.

Hartog, R., and S. Schwartz (2001), Depth-dependent mantle anisotropy below the San Andreas Fault system: Apparent splitting parameters and waveforms, *J. Geophys. Res.*, *106*, 4155–4167, doi:10.1029/2000JB900382.

Hearn, T. M. (1996), Anisotropic *Pn* tomography in the western United States, *J. Geophys. Res.*, *101*, 8403–8414, doi:10.1029/96JB00114.

Humphreys, E. D. (2008), Cenozoic slab windows beneath the western United States, in *Ores and Orogenesis: Circum-Pacific Tectonics, Geologic Evolution, and Ore Deposits*, edited by J. E. Spencer and S. R. Titley, *Ariz. Geol. Soc. Dig.*, *22*, 389–396.

Jousselin, D., and D. Mainprice (1998), Melt topology and seismic anisotropy in mantle peridotites of the Oman ophiolites, *Earth Planet. Sci. Lett.*, *164*, 553–568, doi:10.1016/S0012-821X(98)00235-0.

Kendall, J. M., and P. G. Silver (1998), Investigating causes of D″ anisotropy, in *The Core-Mantle Boundary Region*, *Geodyn. Ser.*, vol. 28, edited by M. Gurnis et al., pp. 97–118, AGU, Washington, D. C.

Kennett, B. L. N., and E. R. Engdahl (1991), Traveltimes for global earthquake location and phase identification, *Geophys. J. Int.*, *105*, 429–465, doi:10.1111/j.1365-246X.1991.tb06724.x.

Li, X. (2007), The lithosphere-asthenosphere boundary beneath the western United States, *Geophys. J. Int.*, *170*, 700–710, doi:10.1111/j.1365-246X.2007.03428.x.

Lin, F. C., M. H. Ritzwoller, and R. Snieder (2009), Eikonal tomography: Surface wave tomography by phase-front tracking across a regional broad-band seismic array, *Geophys. J. Int.*, *177*, 1091–1110, doi:10.1111/j.1365-246X.2009.04105.x.

Liu, Y., S. Crampin, and I. Main (1997), Shear-wave anisotropy: Spatial and temporal variations in time delays at Parkfield, central California, *Geophys. J. Int.*, *130*, 771–785, doi:10.1111/j.1365-246X.1997.tb01872.x.

Liu, Y., H. Zhang, C. Thurber, and S. Roecker (2008), Shear wave anisotropy in the crust around the San Andreas Fault near Parkfield: Spatial and temporal analysis, *Geophys. J. Int.*, *172*, 957–970, doi:10.1111/j.1365-246X.2007.03618.x.

Mainprice, D. (2000), The estimation of seismic properties of rocks with heterogeneous microstructures using a local cluster model—Preliminary results, *Phys. Chem. Earth*, *25*, 155–161, doi:10.1016/S1464-1895(00)00025-9.

Mainprice, D., and P. G. Silver (1993), Interpretation of *SKS*-waves using samples from the subcontinental lithosphere, *Phys. Earth Planet. Inter.*, *78*, 257–280, doi:10.1016/0031-9201(93)90160-B.

Mainprice, D., G. Barruol, and W. Ben Ismail (2000), The seismic anisotropy of the Earth's mantle: From single crystal to polycrystal, in *Earth's Deep Interior: Mineral Physics and Tomography From the Atomic to the Global Scale*, *Geophys. Monogr. Ser.*, vol. 117, edited by S. Karato et al., pp. 237–264, AGU, Washington, D. C.

Mainprice, D., A. Tommasi, H. Couvy, and P. Cordier (2005), Pressure sensitivity of olivine slip systems and seismic anisotropy of Earth's upper mantle, *Nature*, *433*, 731–733, doi:10.1038/nature03266.

Mainprice, D., A. Tommasi, D. Ferre, P. Carrez, and P. Cordier (2008), Predicted glide systems and crystal preferred orientations of polycrystalline silicate Mg-perovskite at high pressure: Implications for the seismic anisotropy in the lower mantle, *Earth Planet. Sci. Lett.*, *271*, 135–144, doi:10.1016/j.epsl.2008.03.058.

McNamara, D. E., and T. J. Owens (1993), Azimuthal shear wave velocity anisotropy in the Basin and Range province using Moho *Ps* converted phases, *J. Geophys. Res.*, *98*, 12,003–12,017, doi:10.1029/93JB00711.

Meade, C., P. G. Silver, and S. Kaneshima (1995), Laboratory and seismological observations of lower mantle isotropy, *Geophys. Res. Lett.*, *22*, 1293–1296, doi:10.1029/95GL01091.

Melbourne, T., and D. V. Helmberger (2001), Mantle control of plate boundary deformation, *Geophys. Res. Lett.*, *28*, 4003–4006, doi:10.1029/2001GL013167.

Mooney, W., and C. S. Weaver (1989), Regional crustal structure and tectonics of the Pacific coastal states: California, Oregon and Washington, in *Geophysical Framework of the Continental United States*, edited by L. C. Pakiser and W. D. Mooney, *Mem. Geol. Soc. Am.*, *172*, 129–161.

Nicolas, A., and N. I. Christensen (1987), Formation of anisotropy in upper mantle peridotites—A review, in *Composition, Structure, and Dynamics of the Lithosphere-Asthenosphere System*, *Geodyn. Ser.*, vol. 16, edited by K. Fuchs and C. Froidevaux, pp. 111–123, AGU, Washington, D. C.

Ozalaybey, S., and M. K. Savage (1994), Double-layer anisotropy resolved from *S* phases, *Geophys. J. Int.*, *117*, 653–664, doi:10.1111/j.1365-246X.1994.tb02460.x.

Ozalaybey, S., and M. K. Savage (1995), Shear wave splitting beneath the western United States in relation to plate tectonics, *J. Geophys. Res.*, *100*, 18,135–18,149, doi:10.1029/95JB00715.

Parsons, T., and P. E. Hart (1999), Dipping San Andreas and Hayward faults revealed beneath San Francisco Bay, *Calif. Geol.*, *27*, 839–842, doi:10.1130/0091-7613(1999)027<0839:DSAAHF>2.3.CO;2.

Pera, E., D. Mainprice, and L. Burlini (2003), Petrophysical properties of the upper mantle beneath the Torre Alfina area (northern Apennines, central Italy), *Tectonophysics*, *370*, 11–30, doi:10.1016/S0040-1951(03)00175-6.

Peselnick, L., A. Nicolas, and P. R. Stevenson (1974), Velocity anisotropy in a mantle peridotite from the Ivrea Zone: Application to upper mantle anisotropy, *J. Geophys. Res.*, *79*, 1175–1182, doi:10.1029/JB079i008p01175.

Polet, J., and H. Kanamori (2002), Anisotropy beneath California: Shear wave splitting measurements using a dense broadband array, *Geophys. J. Int.*, *149*, 313–327, doi:10.1046/j.1365-246X.2002.01630.x.

Savage, M. K. (1999), Seismic anisotropy and mantle deformation: What have we learned from shear wave splitting?, *Rev. Geophys.*, *37*, 65–106, doi:10.1029/98RG02075.

Severinghaus, J., and T. Atwater (1990), Cenozoic geometry and thermal condition of the subducting slabs beneath western North America, in *Basin and Range Extensional Tectonics Near the Latitude of Las Vegas*, edited by B. Wernicke, *Mem. Geol. Soc. Am.*, *176*, 1–22.

Sieminski, A., Q. Y. Liu, J. Trampert, and J. Tromp (2007), Finite-frequency sensitivity of surface waves to anisotropy based upon adjoint methods, *Geophys. J. Int.*, *168*, 1153–1174, doi:10.1111/j.1365-246X.2006.03261.x.

Silver, P. G. (1996), Seismic anisotropy beneath the continents: Probing the depths of geology, *Annu. Rev. Earth Planet. Sci.*, *24*, 385–432, doi:10.1146/annurev.earth.24.1.385.

Silver, P. G., and W. W. Chan (1991), Shear wave splitting and subcontinental mantle deformation, *J. Geophys. Res.*, *96*, 16,429–16,454, doi:10.1029/91JB00899.

Silver, P. G., and W. E. Holt (2002), The mantle flow field beneath western North America, *Science*, *295*, 1054–1057, doi:10.1126/science.1066878.

Silver, P. G., and M. K. Savage (1994), The interpretation of shear-wave splitting parameters in the presence of two anisotropic layers, *Geophys. J. Int.*, *119*, 949–963, doi:10.1111/j.1365-246X.1994.tb04027.x.

Soedjatmiko, B., and N. I. Christensen (2000), Seismic anisotropy under extended crust: Evidence from upper mantle xenoliths, Cima volcanic field, California, *Tectonophysics*, *321*, 279–296, doi:10.1016/S0040-1951(00)00070-6.

Teyssier, C., and B. Tikoff (1998), Strike-slip partitioned transpression of the San Andreas Fault system: A lithospheric-scale approach, in *Continental Transpressional and Transtensional Tectonics*, edited by R. Holdsworth, R. E. Strachan, and R. A. Dewey, *Geol. Soc. Spec. Publ.*, *135*, 143–158, doi:10.1144/GSL.SP.1998.135.01.10.

Titus, S. J., L. G. Medaris, H. F. Wang, and B. Tikoff (2007), Continuation of the San Andreas Fault system into the upper mantle: Evidence from spinel peridotite xenoliths in the Coyote Lake basalt, central California, *Tectonophysics*, *429*, 1–20, doi:10.1016/j.tecto.2006.07.004.

Tommasi, A., B. Tikoff, and A. Vauchez (1999), Upper mantle tectonics: Three-dimensional deformation, olivine crystallographic fabrics and seismic properties, *Earth Planet. Sci. Lett.*, *168*, 173–186, doi:10.1016/S0012-821X(99)00046-1.

Van der Lee, S., and G. Nolet (1997), Seismic image of the subducted trailing fragments of the Farallon plate, *Nature*, *386*, 266–269, doi:10.1038/386266a0.

Walker, K. T., G. H. R. Bokelmann, S. I. Klemperer, and G. Bock (2005), Shear-wave splitting around the Eifel hotspot: Evidence for a mantle upwelling, *Geophys. J. Int.*, *163*, 962–980, doi:10.1111/j.365-246X.2005.02636.X.

Wallace, R. E. (1990), The San Andreas Fault system, California, *U.S. Geol. Surv. Prof. Pap.*, *1515*, 283 pp.

Wookey, J., M. Kendall, and G. Barruol (2002), Mid-mantle deformation inferred from seismic anisotropy, *Nature*, *415*, 777–780, doi:10.1038/415777a.

Wüstefeld, A., G. H. R. Bokelmann, C. Zaroli, and G. Barruol (2008), SplitLab: A shear-wave splitting environment in Matlab, *Comput. Geosci.*, *34*(5), 515–528, doi:10.1016/j.cageo.2007.08.002.

Wüstefeld, A., G. H. R. Bokelmann, G. Barruol, and J. P. Montagner (2009), Identifying global seismic anisotropy patterns by correlating shear-waves splitting and surface waves data, *Phys. Earth Planet. Inter.*, *176*, 198–212, doi:10.1016/j.pepi.2009.05.006.

G. Barruol, G. H. R. Bokelmann, and M. Bonnin, Géosciences Montpellier, Université Montpellier II, CC. 060 Place Eugene Bataillon, F-34095 Montpellier CEDEX 5, France. (barruol@gm.univ-montp2.fr; goetz.bokelmann@gm.univ-montp2.fr; bonnin@gm.univ-montp2.fr)